Proceedings of the ASME 2013 Dynamic Systems and Control Conference
DSCC2013
October 21-23, 2013, Palo Alto, California, USA

DSCC2013-3865

FLATNESS-BASED OPEN LOOP COMMAND TRACKING FOR QUASISTATIC MICROSCANNERS

Klaus Janschek

Institute of Automation, Faculty of Electrical and Computer Engineering,
Technische Universität Dresden, Dresden, Germany
klaus.janschek@tu-dresden.de

Richard Schroedter
Thilo Sandner
Fraunhofer Institute for Photonic Microsystems (FhG-IPMS), AMS, Microscanner R&D,
Dresden, Germany
thilo.sandner@ipms.fraunhofer.de

ABSTRACT

This paper describes a nonlinear command tracking scheme for an electrostatic laser scanning micromirror assembly. The results are based on an innovative gimballed comb transducer concept developed at the Fraunhofer Institute for Photonic Microsystems. The outer mirror axis is designed as a Staggered Vertical Comb (SVC) in out-of-plane configuration and it shall provide a quasistatic operation with large deflection angles for triangular trajectories. The challenges for trajectory design and open loop command tracking are determined by the inherently nonlinear transducer characteristics and the lightly damped mass-spring dynamics. In this paper a flatness-based trajectory design is presented that considers the nonlinear transducer dynamics as well as the nonlinear elastic mechanical suspension with model parameters derived from ANSYS analysis. The paper discusses design constraints and detailed design considerations and it shows proof of concept performance results based on experimental verification with a real microscanner assembly.

INTRODUCTION

Micromachined scanning systems show particular advantages for compactness and fast scanning dynamics. In this context electrostatically actuated comb structures have shown to be appropriate from the MEMS technology point of view (MEMS – micro-electro-mechanical systems). The Fraunhofer Institute for Photonic Microsystems (FhG-IPMS) has developed an innovative laser scanning 2D-micromirror assembly based on a two-stage gimballed electrostatic comb transducer [1,2]. The inner cardanic axis is operating in resonant-mode at 1600 Hz whereas the outer axis is formed by a vertical comb structure in a so-called Staggered Vertical Comb (SVC) configuration that allows quasistatic operation with large deflection angles, typ. ±10°, see Fig.1. A micromirror with elliptic aperture of 2.6x3.6 mm^2 is mounted on the inner axis silicon plate. The micromirror assembly forms the core element of a novel 3D time-of-flight (TOF) laser camera with foveation properties for robotic applications [3]. In the current design the foveated imaging, i.e. higher image resolution at specific regions of interest, is realized by adapting the scanning speed of the outer gimbal axis within a range of typ. 10 Hz, well below the outer axis eigenfrequency of typ. 125 Hz.

From the mechatronic point of view, the command tracking of the quasistatic micromirror axis is challenged by the inherently nonlinear transducer characteristics and the extremely lightly damped mass-spring dynamics. The low mechanical (viscous) damping is due to MEMS-technological constraints and highly desired for the resonant stage. Nevertheless for quasistatic operation, low damping is seen rather as an annoying disturbance that needs special attention for command trajectory design.

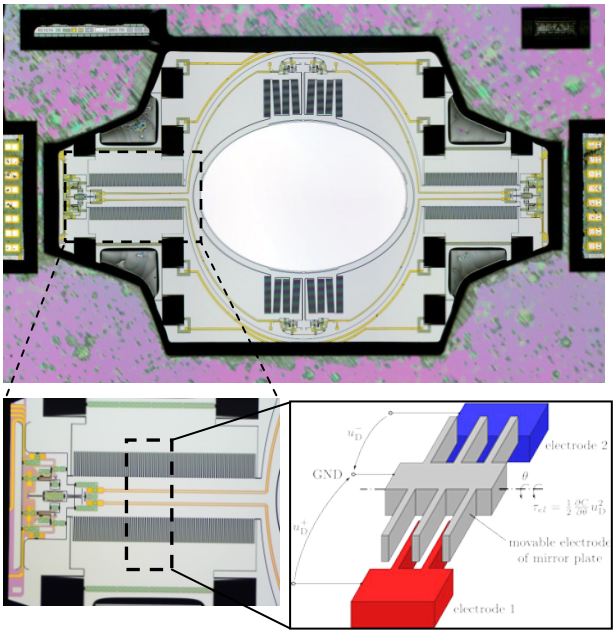

FIGURE 1. GIMBALLED 2D-MICROSCANNER WITH RESONANT DRIVEN MIRROR (INNER AXIS) AND A QUASI-STATIC DRIVEN FRAME (OUTER AXIS)

Closed loop control is used rarely for such MEMS-devices, mainly for technological simplicity, i.e. for avoiding additional sensing devices [4,5]. Although the current micromirror assembly is prepared with piezoresistive position sensors, they are not considered for the design discussed in this paper. Therefore *open loop* control concepts are investigated further. In general open loop control solutions rely fundamentally on appropriate and representative models of transducer dynamics. A well known commanding technique using linear model dynamics is *input shaping*, where the lightly damped eigenmode oscillations are smoothed out by destructive interference of pulse-shaped command inputs [6-9]. Another rather straightforward approach is *prefiltering* of the commanded trajectory profiles by some compensating prefilter with inverse microscanner dynamics [10,11]. Both methods, input shaping and prefiltering, have been investigated further for the current microscanner in [12,13] using a linear design model (input shaping) and a linear compensating prefilter with deflection dependent parameters (adaptive prefilter). Both "linear" solutions show a moderate performance with still some residual oscillations due to imperfect cancellation of the nonlinear mass-spring microscanner dynamics. Further investigations with nonlinear command tracking methods have been done for improvement of the control performance. In this context the *flatness-based* design paradigm [14] is a promising candidate that has been applied to some MEMS applications, e.g. [15], but has not yet been implemented on the kind of MEMS microscanners investigated here. Preliminary results for the flatness-based microscanner design are reported in [13] and are elaborated in more detail in this paper.

The current paper is organized as follows: succeeding this introductory section the nonlinear microscanner design model is presented, followed by detailed design considerations for the flatness-based command generation and completed by experimental results from proof-of-concept tests with the implemented flatness-based control law on a real microscanner assembly.

DESIGN MODEL

The outer quasistatic microscanner axis forms an elastically suspended electrostatic comb transducer, discussed in detail in [11] and schematically shown in Fig. 1, bottom right. The movable comb electrode with deflection angle θ is connected with the substrate by a (nonlinear) torsional spring with differential stiffness $k(\theta)$ (rotational mass-spring system). Viscous damping is very small and caused mainly by airflow (solid state damping is negligible for the monocrystalline silicon-based mirror structure). The nonlinear progressive torsional stiffness increases with more than 30% within the nominal deflection range of 10° (Fig. 2, left). The nonlinear spring torque is given by

$$\tau_{spring}(\theta) = \int_0^{\theta} k(\theta')d\theta' \ . \qquad (1)$$

In the current application the comb transducer is driven by a controllable voltage source u_D. The electrostatic driving torque τ_{el} is given by the spatial change of the comb capacitance $C(\theta)$ and the square of the driving voltage as

$$\tau_{el}(\theta, u_D) = \frac{1}{2}\frac{\partial C(\theta)}{\partial \theta} u_D^2. \qquad (2)$$

The ANSYS computed capacitance function $C(\theta)$ is shown in Fig. 2, right, with two interesting properties: a deflection independent stray capacitance $C_0 := C(\theta = 0°) = 80$ pF and some nonlinear behavior around zero deflection. Due to the unipolar torque generation (square of u_D) a second antagonistic comb drive is needed, resulting in two unipolar electrical driving ports with driving voltages u_D^-, u_D^+ (Fig. 1, bottom right). A generic nonlinear electromechanical design model taking into account both combs and the drive current i_D at the comb drive electrical port (Fig. 3) can be formulated as follows

$$\begin{aligned} J_M\ddot{\theta} + b\dot{\theta} + \tau_{spring}(\theta) &= \tau_{el}(\theta, u_D) \\ i_D(\theta, \dot{\theta}, u_D, \dot{u}_D) &= C(\theta)\dot{u}_D + \frac{\partial C(\theta)}{\partial \theta}\dot{\theta}u_D \end{aligned} \qquad (3)$$

with model parameters $J_M = 4.35 \cdot 10^{-12}\,\mathrm{kgm^2}$ for mirror inertia and $b = 3.3 \cdot 10^{-11}$ Nms/rad for viscous damping. The driving voltage u_D is restricted to $\pm 150\ V$.

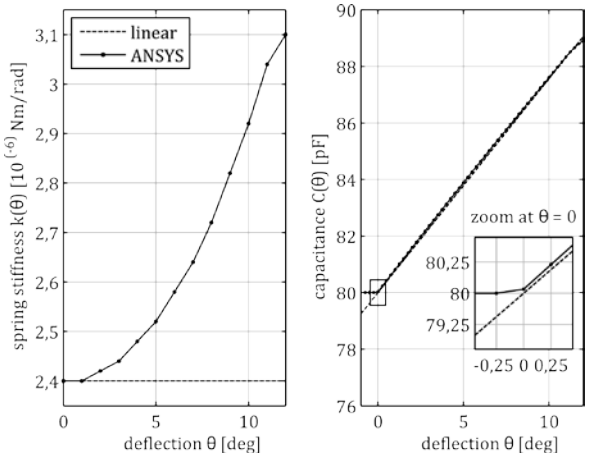

FIGURE 2. NONLINEAR TORSIONAL SPRING STIFFNESS AND COMB CAPACITANCE AS A FUNCTION OF THE MECHANICAL DEFLECTION ANGLE

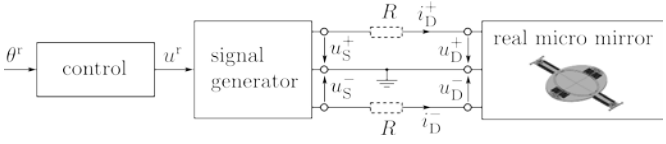

FIGURE 3. SYSTEM BLOCK DIAGRAM WITH ELECTRICAL WIRING

FLATNESS-BASED COMMAND TRAJECTORIES DESIGN

A system block diagram for the open loop control scheme including electrical wiring is shown in Fig. 3. Admissible command (reference) trajectories $\theta^r(t)$ are transformed in drive voltage commands $u^r(t)$ applied at the electrical port(s) of the microscanner. For generation of admissible trajectories $\theta^r(t)$ the *flatness* design paradigm, as introduced in [13], is used that allows a systematic command trajectory design taking into account the nonlinear micro mirror model as given in the previous section.

State Space Model

In the first step the mechanical submodel of Eq. (3) is described as a state space model using the state vector $\boldsymbol{x} = [x_1, x_2] := [\theta, \dot{\theta}]$ and the input $u := u_D$ resulting in

$$\dot{x}_1 = x_2$$
$$\dot{x}_2 = -\frac{b}{J_M} x_2 - \frac{1}{J_M}\int_0^{x_1} k(\tilde{x}_1)\, d\tilde{x}_1 + \frac{1}{2J}\frac{\partial C}{\partial x_1} u^2 \,. \qquad (4)$$

The deflection angle θ defines the output y of the system

$$y := x_1 \,. \qquad (5)$$

Proof of Flatness

Proving the differential flatness property is rather straightforward by choosing the deflection angle θ as *linearizing* or *flat output* z, substituting $[x_1, x_2] = [z, \dot{z}]$ and rearranging Eqs. (4) and (5) in the following way:

$$u = u(z, \dot{z}, \ddot{z}) = \sqrt{\frac{2}{\frac{\partial C}{\partial z}}\left(J\ddot{z} + b\dot{z} + \int_0^z k(\tilde{z})\, d\tilde{z} \right)} \qquad (6)$$
$$y = y(z) = z.$$

Equation (6) says, that the input u, the output y as well as all the state variables may be expressed as algebraic functions of the flat output z and its time derivatives proving differential flatness of the system Eq. (4).

In Eq. (6) the highest time derivatives of the input is $n = 2$ and of the output is $q = 0$. Therefore the *relative degree* r of the system defined by Eq. (3) is $r = n - q = 2$.

Reference Trajectory Design

To compute the input (or control) voltage trajectory for the micro mirror the reference trajectory $z^*(t)$ must be r-times continuously differentiable. Thus the desired linear triangle trajectory will be adapted with smooth polynomials at its reversal points as shown in Fig. 4, where the linear area covers 80% of the total deflection. To ensure second order differentiability with respect to time the polynomials have the form:

$$z^*(t) = \sum_{i=0}^{5} a_i \tau^i(t), \qquad (7)$$

where a_i are constant coefficients, constraint by the interception points at the linear area, and $\tau(t) = (t - t_0)/(t_T - t_0)$ is the normalized time between the start time t_0 and the end time t_T of the reversal polynomial.

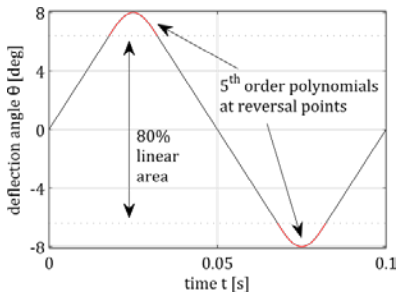

FIGURE 4. SMOOTH REFERENCE TRAJECTORY AS AN ADAPTED TRIANGLE TRAJECTORY WITH POLYNOMIALS

Trajectory Command Voltage

Finally the input voltage trajectory is computed with Eq. (6) using the reference trajectory $z(t)$ as shown in Fig 4. The computation of the partial derivative of the capacitance function in Eq. (6) needs special attention. The ANSYS model in Fig. 2, right, is only a first approximation and $C(\theta)$ cannot be measured directly. As a workaround solution the following indirect reconstruction has been employed. The static deflection relation by equating Eqs. (1), (2) can be easily rearranged to

$$u_D(\theta) = \sqrt{\frac{2\int_0^\theta k(\tilde{\theta})\, d\tilde{\theta}}{\frac{\partial C}{\partial \theta}}} \quad \Rightarrow \quad \frac{\partial C}{\partial \theta} = \frac{2\int_0^\theta k(\tilde{\theta})\, d\tilde{\theta}}{u_D^2} \,. \qquad (8)$$

Using the measured deflection characteristic $\theta(u_D)$ as shown in Fig. 5 allows a straighforward computation of the partial derivative of the capacitance function from Eq. (8). Figure 6 shows this trajectory split for both electrodes of the micro mirror and illustrates the behavior similar to a root function, that requires a fast charge reversal near the zero deflection.

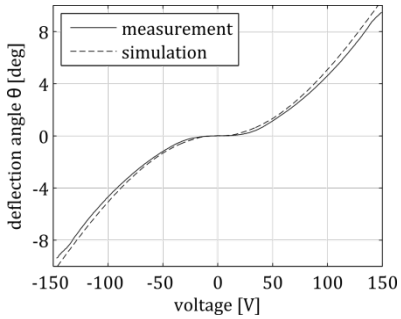

FIGURE 5. STATIC DEFLECTION CHARACTERISTIC CURVE USED TO COMPUTE THE VOLTAGE TRAJECTORY

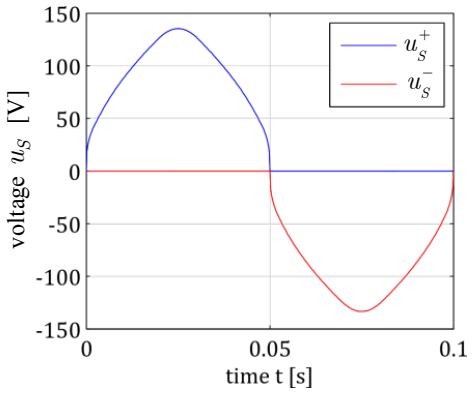

FIGURE 6. TYPICAL TRAJECTORY COMMAND VOLTAGE

EXPERIMENTAL VERIFICATION

Experiment Setup

The experimental verification of the proposed open loop control concept aims in (i) validation of microscanner model accuracy and (ii) performance assessment under operational conditions. The experiments have been conducted with a FhG-IPMS developed microscanner according to Fig. 1 in a test setup shown in Fig. 6. External reference measurement of the real mirror deflection $\theta(t)$ has been done with a position sensitive detector (PSD) setup as sketched in Fig. 7.

The measurement equation for mirror deflection angle $\hat{\theta}(t)$ using the PSD is given as

$$\hat{\theta} = \frac{1}{2}\arcsin\left(\frac{k_{PSD}}{d}\frac{I_a - I_b}{I_a + I_b}\right), \qquad (9)$$

where I_a, I_b are displacement currents, d is the distance between PSD and micro mirror and k_{PSD} is a scaling factor.

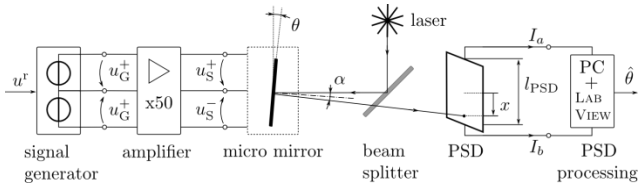

FIGURE 7. EXPERIMENTAL SETUP FOR MEASUREMENT OF MIRROR DEFLECTION ANGLE

Experiment Results

In general the ANSYS models are sufficiently representative, as can be deduced e.g. from the comparison of measured and simulated (ANSYS based) deflection characteristic in Fig. 5. Also the dynamic trajectory tracking performances are rather close to the predicted ones. In Fig. 8 are given typical measured time responses for a 10 Hz flatness-based reference trajectory. Results for the *measured tracking error* (error w.r.t. reference)

$$e_\theta(t) := \theta^r(t) - \hat{\theta}(t) \qquad (10)$$

are shown in Fig. 8b. There can be seen residual oscillations at the micro mirror outer axis eigenfrequency of 123 Hz resulting from inaccuracies of the design parameters.

From the application point of view the foveation function (cf. introductory section) requires a very high *repeatability* of the spatial scanning profile. An appropriate metrics for measuring the repeatability is the *dispersion* as defined in Tab. 1 using the *deviation from the mean deflection*

$$\Delta\overline{\theta}_{\max}(t_i) := \max_{49\ \text{cycles}}\left(\hat{\theta}(t_i) - \operatorname{mean}_{49\ \text{cycles}}\left(\hat{\theta}(t_i)\right)\right) \qquad (11)$$

as baseline metrics.

A summary of measured performance metrics is given in Tab.1. For the evaluation of the performance metrics the 80% operating range of constant scan speed (±6.4° mirror deflection, see Fig. 8a) has been used. The verification shows that with this kind of open loop command tracking operational tracking accuracies of typ. 2% and a high repeatability of about 2‰ for successive scans can be achieved.

Serial Resistance – Impedance Feedback

The dynamic microscanner performance is fundamentally affected by a serial resistance in the electrical driving circuit, see dashed part of Fig. 3. In a positive way such a resistance is realizing an analog electromechanical passive damping of the lightly damped mass-spring mirror dynamics and it is improving considerably dynamic robustness, see the detailed analysis in [11,12]. Considering a resistance R in series the relationship between commanded drive voltage u_S and mirror drive voltage u_D can be written as

$$u_D = u_S - R \cdot i_D \qquad (12)$$

employing nothing else than an analog feedback with "gain" R at the electrical port of the mirror – *impedance feedback*. In [11] it is shown that R can be used as a design parameter for achieving maximum possible damping.

Nevertheless this raises problems for the bipolar operation of the microscanner because of the stray capacitance C_0, see previous section. The square root law Eq. (8) for the driving voltage requires infinite (very large) slope (rate of change) for the driving voltage at zero deflection crossing. In consequence this results in infinite (very large) drive currents due to $i_D = C_0 \dot{u}_D$ and reduces the net voltage at the mirror port (cf. Eq. (12)) and thus not giving full authority to electromechanical torque generation. As a result residual excitation of the mass-spring eigenmode can be observed at deflection zero crossing. This prohibits the direct use of impedance feedback for bipolar operation. We are currently investigating measures at electrical circuit level to compensate for these undesirable load/unload artifacts.

TABLE 1. STATISTICAL RESULTS IN 80% LINEAR DEFLECTION AREA: MEAN ERROR FROM REFERENCE TRAJECTORY AND DISPERSION (REPEATABILITY) FROM 49 TRIANGLE CYCLES CF. FIG 8

Error Type	Metrics	Exp. Result
Error from reference	$\frac{e_{\theta,\max} - e_{\theta,\min}}{12.8°}$	1.82%
Dispersion (Repeatability)	$\frac{\Delta\bar{\theta}_{\max} - \Delta\bar{\theta}_{\min}}{12.8°}$	0.215%

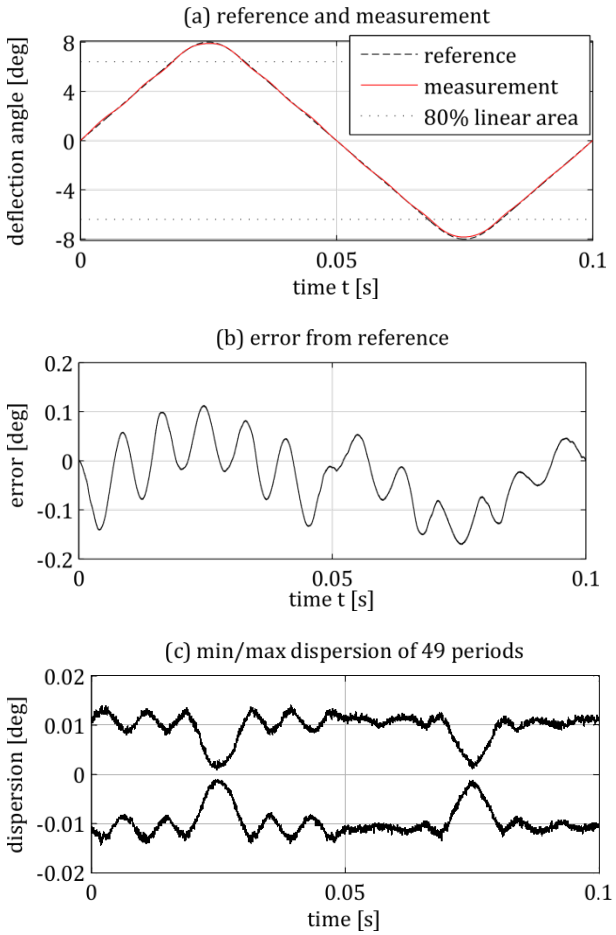

FIG. 8. EXPERIMENTAL RESULTS (FOR ONE PERIOD OF A 10 HZ REFERENCE TRAJECTORY IN STEADY STATE): (A) REFERENCE AND MEASUREMENT, (B) ERROR BETWEEN MEASUREMENT AND REFERENCE, (C) MIN. AND MAX. DISPERSION OF 49 PERIODS REPRESENTING THE REPEATABILITY OF THE RESULT

REFERENCES

[1] Sandner, T., Jung, D., Kallweit, D., Grasshoff, T., Schenk, H., 2011. "Microscanner with Vertical out of Plane Combdrive". *IEEE/LEOS Proc. Int. Conf. on Optical MEMS & Nanophotonics,* 2011, pp. 33-34.

[2] Jung, D., Sandner, T., Kallweit, D., Schenk, H., 2012."Vertical comb drive microscanners for beam steering, linear scanning, and laser projection applications". In: *Proc. SPIE 8252, MOEMS and Miniaturized Systems XI*, 82520U (February 9, 2012); doi:10.1117/12.906690.

[3] Thielemann, J., Sandner, T., Schwarzer, S., Cupcic, U., Schumann-Olsen, H., Kirkhus, T., 2010. „TACO: Three-dimensional Camera with Object Detection and Foveation", *EC FP7 grant no 248623*, http://www.taco-project.eu/

[4] Ferreira, A., Aphale, S.S., 2011. "A Survey of Modeling and Control Techniques for Micro- and Nanoelectromechanical Systems", *IEEE Transactions on Systems, Man, and Cybernetics—Part C: Applications and Reviews*, Vol. 41, No. 3, pp. 350-364.

[5] Borovic, B.; Hong, C.; Zhang, X.M.; Liu, A.Q.; Lewis, F.L., 2005. "Open vs. Closed-Loop Control of the MEMS Electrostatic Comb Drive". *Proceedings of the 2005 IEEE International Mediterrean Conference on Control and Automation*, pp. 982 – 988.

[6] Singer, N.C.; Seering, W.P., 1990. "Preshaping Command Inputs to Reduce System Vibration". *Trans. ASME, J. Dyn. Syst. Meas. Control*, vol. 112, no. 1, 1990, pp. 76–82.

[7] Chen, K.-S.; Ou, K.-S., 2007. "Command-Shaping Techniques for Electrostatic MEMS Actuation: Analysis and Simulation". *Journal of Microelectromechanical Systems,* Volume 16 (2007), Issue 3, pp.537-549.

[8] Schitter, G.; Thurner, Ph.J.; Hansma, P.K., 2008. "Design and input-shaping control of a novel scanner for high-speed atomic force microscopy". *Mechatronics*, Volume 18 (2008), Issues 5–6, pp. 282-288.

[9] Ou, K.-S.; Chen, K.-S.; Yang, T.-S.; Lee, S.-Y., 2011. "Fast Positioning and Impact Minimizing of MEMS Devices by Suppression of Motion-Induced Vibration by Command-Shaping Method". *Journal of Microelectromechanical Systems*, Vol. 20 (2011), No.1, pp. 128 –139.

[10] Zeitz, M., 2012. Feedforward Control Design in the Frequency Domain: Offline or Online (in German), *at - Automatisierungstechnik* 60 (2012), pp. 375-383.

[11] Janschek, K., 2012. Mechatronic Systems Design: Methods, Models, Concepts. Springer.

[12] Janschek, K.; Sandner, T.; Schroedter, R.; Roth, M., 2013. "Adaptive Prefilter Design for Control of Quasistatic Microscanners". Accepted paper, 6th IFAC Symposium on Mechatronic Systems – Mechatronics '13, April 10-12, 2013, Hangzhou, China.

[13] Schroedter, R., Roth, M., Sandner, T., Janschek, K., 2013. Model-based motion tracking for quasistatic microscanners (in German). In: *Proceedings of the Fachtagung Mechatronik 2013*, 6.-8.3.2013, Aachen, Germany, ISBN3-86130-958-0, pp. 141-146.

[14] Fliess, M., Lévine, J. and Rouchon, P. , 1995. "Flatness and defect of nonlinear systems: Introductory theory and examples", *International Journal of Control*, 1995, vol. 61, pp. 1327-1361.

[15] Zhu, G.; Levine, J.; Praly, L.; Peter, Y.-A., 2006. "Flatness-Based Control of Electrostatically Actuated MEMS With Application to Adaptive Optics: A Simulation Study". *J.of Microelectromechanical Systems*, Vol. 15 (2006), Issue 5, pp. 1165-1174.